SYMPOSIUM ARTICLE

The Biomechanics of Multi-articular Muscle–Tendon Systems in Snakes

Henry C. Astley[1]

Departments of Biology and Polymer Science, Biomimicry Research and Innovation Center, The University of Akron, Akron, OH 44325, USA

From the symposium "Long Limbless Locomotors: The mechanics and biology of elongate, limbless vertebrate locomotion" presented at the annual meeting of the Society for Integrative and Comparative Biology January 3–7, 2020 at Austin, Texas.

[1]E-mail: hastley@uakron.edu

Synopsis   The geometry of the musculoskeletal system, such as moment arms and linkages, determines the link between muscular functions and external mechanical results, but as the geometry becomes more complex, this link becomes less clear. The musculoskeletal system of snakes is extremely complex, with several muscles that span dozens of vertebrae, ranging from 10 to 45 vertebrae in the snake semispinalis-spinalis muscle (a dorsiflexor). Furthermore, this span correlates with habitat in Caenophidians, with burrowing and aquatic species showing shorter spans while arboreal species show longer spans. Similar multi-articular spans are present in the prehensile tails of primates, the necks of birds, and our own digits. However, no previous analysis has adequately explained the mechanical consequences of these multi-articular spans. This paper uses techniques from the analysis of static systems in engineering to analyze the consequences of multiarticular muscle configurations in cantilevered gap bridging and compares these outcomes to a hypothetical mono-articular system. Multi-articular muscle spans dramatically reduce the forces needed in each muscle, but the consequent partitioning of muscle cross-sectional area between numerous muscles results in a small net performance loss. However, when a substantial fraction of this span is tendinous, performance increases dramatically. Similarly, metabolic cost is increased for purely muscular multi-articular spans, but decreases rapidly with increasing tendon ratio. However, highly tendinous spans require increased muscle strain to achieve the same motion, while purely muscular systems are unaffected. These results correspond well with comparative data from snakes and offer the potential to dramatically improve the mechanics of biomimetic snake robots.

Introduction

Muscle is the motor of vertebrate movement, and indeed most animal movement. The intrinsic action of muscles is to shorten along the fibers, and converting this shortening to a range of other body motions requires interaction with a skeleton, whether soft/hydrostatic or rigid and jointed. The geometry of these skeletal interactions can have tremendous effects of the relationship between muscle fiber force and motion and the resulting force and motion of the body part. The simplest example is the mechanical advantage of muscles which cross a single joint, with musculoskeletal geometries being geared for either high output speed or force (Smith and Savage 1956). Biarticular muscles such as the human semimembranosus are common within vertebrate limbs, and can play a variety of roles depending on moment arms, activation levels, and the recruitment of other muscles in the limb crossing the distal and proximal joints (Bodine et al. 1982; Van Ingen Schenau 1989; van Ingen Schenau et al. 1994).

The axial musculature of snakes presents a particularly challenging system for understanding the link between musculoskeletal morphology and functional outcome due to the exceptionally multi-articular nature of many muscles (Mosauer 1935; Auffenberg 1962; Gasc 1974, 1981; Pregill 1977; Jayne 1982; Fig. 1). Depending on the muscle group and species, a given muscle may span anywhere from 1 to 45 vertebrae (Mosauer 1935; Auffenberg 1962; Gasc
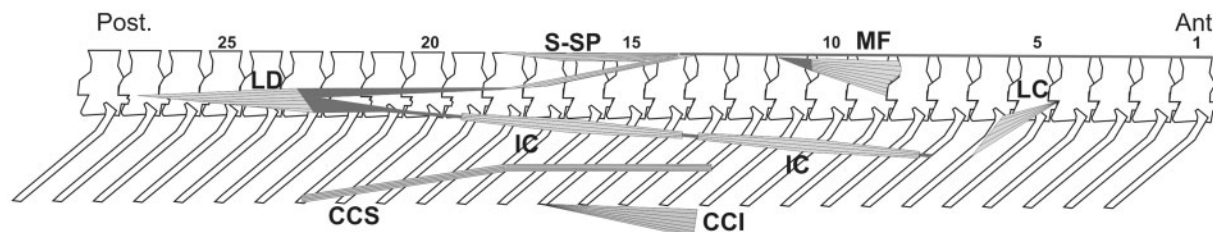
Fig. 1 Diagram of selected snake axial muscles. Each muscle repeats segmentally in overlapping "bands" along the body. Anterior is to the right. Muscle tissue is in light gray with dark lines indicating fiber direction and tendon/connective tissue is in dark gray. Muscles shown: semispinalis-spinalis (SSP), multifidus (MF), longissimus dorsi (LD), iliocostalis (IC), levator costae (LC), and costocutaneous superior (CCS) and inferior (CCI). The CCS and CCI insert onto the skin.

1974, 1981; Pregill 1977; Jayne 1982; Fig. 1). Furthermore, many of the muscles with the largest cross-sectional area and muscle mass, and thus presumably the greatest contribution to performance, have high span and exhibit high variability across species (Ruben 1977; Jayne 1982, 1988a, 1988b; Jayne and Riley 2007; Penning 2018; Fig. 1). Lizards show broadly homologous muscle arrangements with muscles spanning much smaller numbers of segments, though limbless lizards show more snake-like morphology, suggesting this configuration has functional benefits (Auffenberg 1962; Gasc 1974, 1981). The hypothesized functional benefit is further supported by convergent evolution of this multi-articular morphology in other elongate, flexible, segmented systems, notably the prehensile tail of primates (Lemelin 1995) and the neck of birds (van der Leeuw et al. 2001; Boumans et al. 2015; Böhmer et al. 2019), as well as to a much lesser degree in the human finger and erector spinae.

However, the functional consequences of this morphology remain unclear. Detailed anatomical data are available for only a few species and muscles, though descriptive studies have noted trends (Mosauer 1935; Gasc 1974, 1981). Ruben (1977) noted differences in span and the relative proportion of the span which is tendinous in a pair of constricting and non-constricting snakes, and suggested that the shorter, more muscular span of constrictors conveyed advantages in the range of motion while the more tendinous spans of non-constrictors were beneficial for speed. However, the most comprehensive study on this topic was Jayne's (1982) examination of the snake semispinalis-spinalis (SSP) muscle complex (SSP in Fig. 1). The SSP is a large muscle which dorsiflexes the vertebrae when bilaterally active (as in gap bridging and sidewinding [Jayne 1988a; Jorgensen and Jayne 2017]) and contributes to lateral flexion when unilaterally active (during lateral undulation and concertina [Jayne 1988a, 1988b]). This study, and the subsequent phylogenetic re-analysis (Tingle et al. 2017), showed that the SSP varied extensively within Caenophian snakes and correlated strongly with habitat and constriction (Jayne 1982; Tingle et al. 2017). Highly arboreal snakes displayed very long and tendinous spans of the SSP while terrestrial, burrowing, and aquatic habitats were correlated with shorter and more muscular spans (Jayne 1982; Tingle et al. 2017). While the number of species is lower, similar functional links have been found in primate tails and bird necks (Lemelin 1995; Böhmer et al. 2019).

Despite these correlations, the mechanical consequences of these systems has remained obscure. Work on human finger and erector spinae muscles has taken advantage of the well-described morphology and minimal variability by using detailed models of the anatomy to determine exact solutions (Macintosh et al. 1993; Tveit et al. 1994; Fowler et al. 2001; Pollard and Gilbert 2002; Daggfeldt and Thorstensson 2003), which makes sense given the highly limited anatomical variability of these system but which cannot produce generalized insights which apply interspecfically. The striking multi-articular morphology of snake muscle has attracted attention from the robotics community as well. Inoue et al. (2010) performed simulations and designed a wheeled snake-inspired robot, but did not evaluate the results of either beyond noting qualitative similarity with the motion of biological snakes; similarly, a simulation study by Faraji and Barazandeh (2012) also showed only that the system could generate sinusoidal motion. Our best insight into the consequences of multi-articular morphology comes from a modeling study of lateral undulation, showing that for as muscle span increased from 1 to 5, the overall locomotor speed increased and summed muscular force decreased (Kano et al. 2011). While most snake muscles span considerably higher numbers of segments, this study provides a strong indication that multi-articular muscles provide substantial locomotor benefits, though the paper did not assess the detailed mechanics at the individual muscle level, the consequences of tendons, or metabolic cost
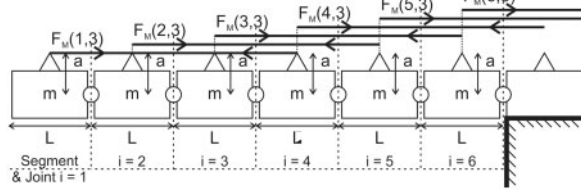
Fig. 2 Diagram of model system with a cantilever length of $N = 6$ and a multi-articular span of $p = 3$. Anterior is to the left, and segment 7 is anchored to the substrate. Segments have a mass m and a length L. A single muscle originates on each vertebra and applies uniform tension along its length ($F_M(i, p)$); all muscles have the same lever arm (a), but have been offset for visual clarity (dotted lines). Joints are numbered by their prior segment and muscles are numbered according to the number of the anterior segment.

(Kano et al. 2011). Rezaei et al. (2010) attempted to model a single highly multi-articular muscle spanning numerous joints using inverse dynamics methods, and suggested that increased span reduced the required tension in this single muscle. However, the initial inverse dynamics solution included torsional springs at the joints and friction between the muscle and its constraints, but the spring constant and frictional coefficient were set to zero later in the derivation to simplify the subsequent computations Rezaei et al. (2010)(and, presumably, to more closely resemble the highly flexible vertebral column of biological snakes). This produced a system in which there were multiple joints but only a single constraint (muscle length), allowing the system to adopt a wide variety of combinations of dorsal and ventral joint deflections to meet this constraint. When in a cantilevered position, as in a snake bridging a gap between trees, the system will collapse into the joint configuration with the lowest potential energy, typically accomplished by ventral flexion of the posterior joints nearest the anchor point and compensatory dorsiflexion of the distal vertebrae to accommodate the constraint of the muscle length (see proof in the Supplementary Material and demonstration in Supplementary Video S1). This failure mode shows that the 1:1 correspondence of snake muscle segments to vertebrae is not only a consequence of a fundamentally metameric body plan (though this doubtless plays a role), but a mechanical necessity to provide equal or greater constraints than the degrees of freedom available. Attempts by the authors to mechanically verify their calculations produced conflicting results (Rezaei et al. 2010).

In order to arrive at generalized insights for multi-articular systems, I will use a mathematical model of the SSP muscle to investigate the consequences of muscular and tendinous span on horizontal cantilevered gap bridging in snakes (Fig. 2). This behavior is an ideal starting point as electromyographic evidence shows that the SSP is strongly active during cantilevered gap bridging (Jorgensen and Jayne 2017), as well as strong interspecific differences in SSP span and tendon ratio (Jayne 1982; Tingle et al. 2017) and animal performance (Lillywhite et al. 2000; Ray 2012). I will model both the maximum gap crossed and the metabolic cost. I hypothesize that increasing total span and tendon ratio will increase both performance metrics, at the cost of range of motion.

Methods

Assumptions

This paper uses several assumptions and simplifications to make the system analytically tractable.

(1) I assume a static or quasi-static posture, in which accelerations are minimal and inertia can therefore safely be neglected; this corresponds well to the observed gap bridging behavior of snakes, in which movements are slow, with slight vertical oscillations apparent only near maximal performance (Jayne and Riley 2007).

(2) I do not include the head or cervical musculature (Fig. 2). These could easily be added via the methods below, but would add an additional variable to account for and would only add an additional linear term to the external moment equation (Equation (1)). Furthermore, only limited descriptions are available of the cervical muscular anatomy (Pregill 1977). Thus, explicit incorporation of the head and cervical musculature is left to future work.

(3) All intervertebral joints are assumed to be frictionless (consistent with their synovial anatomy [Winchester and Bellairs 2009]) and capable of resisting all axial and shear loads applied, thus restricting our concern to the moment at each intervertebral joint.

(4) I consider only a single muscle, the SSP, and do not consider the potential contributions of other dorsiflexors such as the multifidus (Mosauer 1935; Gasc 1981; Jayne and Riley 2007; Fig. 2). While these muscles are likely to contribute, the addition of a parallel muscle precludes partitioning activation and force generation between them, rendering the equations indeterminate without simplifying assumptions (Winter 2009), many of which are potentially dubious in a system as sparsely studied as snake biomechanics.

(5) I assume that only one muscle originates from each vertebrae and inserts on one vertebra

(Fig. 2). This is a simplification of the snake anatomy, particularly for the posterior insertion, which may span two to three vertebrae (Mosauer 1935; Gasc 1981; Jayne 1982). Combined with the second assumption (no head or cervical musculature), this means that the most anterior joint will be crossed only by a single muscle, while the second joint will be crossed by two (if the span ≥ 2) and so on (Fig. 2).

(6) I assume that all segments are identical in length, mass, and muscle lever arm (Fig. 2). While the vertebrae of snakes vary in dimensions longitudinally (and thus presumably also in mass) (Johnson 1955; Mccartney 2013), this simplification is necessary to render the equations tractable and to avoid additional complicating terms. Again, future analysis can make these term (m, L, and a below) functions of joint number to more closely match biological reality, but I predict that for biological plausible functions of these terms the overall conclusions of this paper will remain valid.

Model

The model of the system is represented in Fig. 2, though limited to only six segments for visual clarity. Each segment has a mass (m) and a length (L), connected by a series of joints numbered (i) according to the anterior segment; thus joint $i = 1$ is between the first and second segment, joint $i = 2$ is between the second and third, etc. Muscles will be designated according to the number of the anterior segment which they originate on, for example, the muscle originating on the first segment is muscle 1, regardless of how many vertebrae it spans before the posterior insertion (Fig. 2). The number of vertebrae spanned by a muscle is designated as p, and as a consequence, the number of muscles crossing a given joint will increase from 1 to p for the anterior joints $1 < i \leq p$, after which each joint will be spanned by p muscles, and the force of each muscle will be the function $F_M(i, p)$ (Fig. 2). All muscles function at the same lever arm (a), though they are offset for clarity in Fig. 2.

Method of sections

As the system is quasi-static, I can employ the section "method of sections," a mathematical practice widely used in the analysis of static structures in engineering (Bedford et al. 1997). For a static system with known loads, one can take an imaginary, continuous "slice" through the structure which cuts N elements, defining a force variable (F_1, F_2, ..., F_N) for the tension/compression force of each member (which must be parallel to this member). Because

the system is static, the summed forces in both horizontal and vertical directions must be equal to zero, as are the summed moments about a given point, which allows us to create a system of equations. For small N, the system will be solvable, but if not, different sections crossing some (but not all) of the first set of beams will result in still more equations. For systems with more unknowns than equations, additional simplifying assumptions can be used (such as minimal strain energy), but those will not be necessary for this study. In this case, a section passing through joint $i = 1$ crosses two structures, the joint itself (the location of the gravitational moment), and the muscle, which generates a counteracting torque via its tension and the lever arm (a) such that the net moment is zero (otherwise the system would not be static). At joints 2 and higher, sections cross additional muscles and joints (which are subject to different gravitational moments), but can be solved based on calculations at prior joints (see below).

The analysis method outlined will first be used to compute the force in each individual muscle segment via the method of sections and to derive a continuous function which approximates these forces. Forces will be expressed in terms of three key variables: the anterior origin of the muscle (i), the multi-articular muscular span (p), consisting of the number of joints spanned from anterior to posterior attachment and the tendon ratio (t), defined as the fraction of the multi-articular span which is tendinous (0 being purely muscular and 1 being purely tendinous). Three performance metrics will be used: maximum gap spanned, metabolic energy consumption, and range of motion.

Maximum gap bridging performance

The finding that the muscles crossing a given joint are not contributing equally to the required force, and that more posterior muscles contribute more than anterior ones (Equations (4), (6), and (7), Fig. 3), leads directly to the criterion which determines the maximal horizontal cantilever length. Rather than failing when the required force exceeds the combined maximum force of all muscles crossing a given joint, failure will occur when the force which must be contributed by a given muscle at a given joint exceeds the maximal force which it is physiologically capable of contributing. This critical force will be determined by the maximum available muscle cross-sectional area, CSA_{Max} multiplied by the peak isometric muscle stress, P_0 (typically ~ 30 N/cm^2 in vertebrates). All else being equal, higher maximal cross-sectional area will result in longer gap bridging. However, when considering the effect of multi-

articular muscle morphology, the effect increase in muscle span must not be confounded by simultaneously increasing available cross-sectional area; if each muscle is assumed to have a fixed cross-sectional area regardless of span, a snake with a span of 40 would have 40 times the total cross-sectional area and 40 times the muscle mass of a mono-articular snake! Instead, for snake of a fixed length and SSP muscle mass, and thus a fixed total cross-sectional area at any given joint, CSA_{Max}, increasing the span will require subdividing that cross-section area across the muscles spanning that joint. Thus, the maximum cross sectional area available to a given muscle will be CSA_{Max} divided by the span, and the peak force will be this area multiplied by P_0.

However, the SSP is highly tendinous, particularly in arboreal species (Jayne 1982; Tingle et al. 2017), and these tendons have a small cross-sectional area compared with muscles (which can be neglected for the purposes of these calculations). As a result, the muscle can span many segments without nearly as much loss of cross-sectional area if it is tendinous. To formalize this, I introduce the tendon ratio (t) denoting the proportion of the multi-articular span which is tendinous. Thus, for a span of p, the tendinous portion will span $t * p$ vertebral joints and the muscular section will span $(1-t) * p$ vertebral joints. However, certain combinations of t and p will produce unrealistic results, particularly those which would result in muscular segments lengths shorter than a single segment, as this would falsely inflate the available cross-sectional area beyond what is available for a single segment of the snake's body. Correspondingly, all data for which the condition $(1-t) * p \geq 1$ is violated are excluded. I will evaluate the consequences of both purely muscular multi-articular span (p, $t = 0$) and tendinous multi-articular span on gap bridging performance, relative to a system with no tendon and mono-articular muscles.

I will also examine the effects of increased segment length on gap bridging performance. The consequences of increasing segment length are more complex, as doing so will increase the moment arm of each segment and thus the gravitational moment at each joint, but will also allow the snake to achieve greater absolute cantilever distances with the same number of joints, or the same distance with fewer joints. Absolute performance will be the performance metric in this analysis, defined as the number of joints (i) multiplied by the segment length L.

Metabolic cost

While maximum performance is often a key metric in biological systems, the metabolic cost of behaviors can also be relevant, particularly for species like snakes, which are often specialized for a low-energy lifestyle. While precise predictions of the absolute metabolic cost of this behavior would require a far more detailed model of snake muscle physiology than currently possible, particularly given the absence of all but the simplest measures of muscle physiology for any snake, this metric can still be explored with some simplifications. Because force must be maintained along the entire length of the muscle, the metabolic cost of a muscle will increase with fiber length, and thus be proportional to total active muscle volume (Biewener and Roberts 2000). However, tendon is a passive tissue, requiring no metabolic input to carry load, thus only the muscular volume is considered. This volume will be multiplied by an unknown constant, Q, representing the cost per unit volume of an isometric contraction. The key metric will be the metabolic cost savings, defined as the difference between a mono-articular, purely muscular system and a system with a given p and t, divided by the cost of the mono-articular, purely muscular system. Values greater than 0 represent the proportion of metabolic cost savings (e.g., 0.5 indicates a 50% reduction in cost). Metabolic cost savings will be assessed in terms of the consequences of multi-articular span (p) and tendon ratio (t). As previously, all data for which the condition $(1-t) * p \geq 1$ is violated are excluded.

Range of motion

I will also quantify the effect of multi-articular span and tendon ratio on range of motion. Muscle is limited in both the relative length change it can undergo and the speed with which it can do so. While tendon can change length (e.g., elastic energy storage for energy conservation or power amplification), these changes are typically very small relative to the length change in muscle, and will be neglected for the purposes of this paper.

Mechanical testing

In order to test the validity of the muscle force equations, I constructed a simple mechanical model for a system with a span of four ($p = 4$), consisting of 3D printed segments joined with vertically oriented 4 mm miniature barrel hinges, each with a pair of screw eyelets to constrain "muscle" movement (the same model as in Supplementary Video S1). To determine force, Kevlar thread was tied to the anterior eyelet on the first segment, threaded through the remaining eyelets in the span, then attached to a Pesola spring scale (various models to

accommodate differences in force) held parallel to the line of action. The model was then positioned so that the joint was cantilevered and the force on the spring scale recorded (lowest of three attempts). The Kevlar thread was then tied at the posterior attachment point appropriate for the span (in the case of the first "muscle", at segment 5) at a length which allowed it to remain taught. This process was then repeated sequentially for each of the posterior segments for a total of seven measurements; beyond this point, imprecisions in the hinges and attachment locations caused the system to "lock up" due to small lateral forces. Forces are compared with those predicted from derivations. Because the model is only seven segments, the exact calculation (Equation (4)) is preferred, as the continuous approximation equation (7) suffers from inaccuracies at small values of i and p.

Results

Muscular force calculations

For a beam consisting of discrete segments connected by joints, as in our model of a horizontally cantilevered snake (Fig. 2), the external moment M_{Ext} at any joint will be

$$M_{Ext}(i) = (m * g * i) * \frac{L * i}{2} = \frac{m * g * L * i^2}{2}, \quad (1)$$

where m is the mass of a single segment, L is the length of a single segment, g is the acceleration due to gravity, and i is the number of the joint from most anterior (Equation (1)) to most posterior (N) (Fig. 2). This equation corresponds well with the equation for a solid cantilevered beam under uniform loading (Bedford et al. 1997). For the snake to hold a static position, it must counteract $M_{Ext}(i)$ at each joint i through some combination of muscles acting across the joint (Fig. 2). Since all muscles have the same moment arm a (see Assumptions, Fig. 2), the sum of all muscular force at a given joint (F_{Mtotal}) is

$$0 = M_{Ext}(i) - a * \sum F_M$$
$$\therefore \sum F_M = F_{Mtotal}(i) = \frac{M_{Ext}(i)}{a} = \frac{m * g * L * i^2}{2 * a}.$$

In the simplest case of the muscular span $p = 1$, because each joint is spanned by only a single muscle, this muscle is solely responsible for counteracting the external moment at that joint and thus $F_M(i, 1) = F_{Mtotal}(i)$. This system will serve as our baseline for future comparison. For $p > 1$, in all cases, the first joint is spanned only by a single muscle, and thus $F_M(1, p) = F_{Mtotal}(1)$. However, the second joint is spanned by two muscles (Fig. 2), each of which contribute to the summed muscular force

($F_{Mtotal}(i)$). Because the tension in a muscle must be equal at all points along its length, $F_M(1, p)$ is known from the prior calculation, thus $F_M(2, p) = F_{Mtotal}(2) - F_M(1, p)$. For $p \geq 3$, the third joint is spanned by three muscles (Fig. 2), and with $F_M(1, p)$ and $F_M(2, p)$ constrained by prior joints, $F_M(3, p) = F_{Mtotal}(3) - F_M(2, p) - F_M(1, p)$. Indeed, for all $i \leq p$ and for all p, $F_M(i, p)$ must only add enough force to compensate for the increase from $F_{Mtotal}(i-1)$ to $F_{Mtotal}(i)$, which simplifies to

$$\text{for } i \leq p, \ F_M(i, p) = F_{Mtotal}(i) - F_{Mtotal}(i-1)$$
$$\therefore F_M(i, p) = \frac{m * g * L}{2 * a} * (2i - 1) = C_M * F_F$$
$$\text{where } C_M = \frac{m * g * L}{2 * a} \ \& \ F_F = 2i - 1$$

At this point, it becomes convenient to talk about the equation into two parts, consisting of a "morphological coefficient" (C_M) which includes all of the constant terms defined by the geometry of the system (mass, length, gravity, and lever arm) and a "force function" (F_F), which determines the value which the morphological coefficient is multiplied by to determine total force for a given muscle, based on joint number and muscle span. As seen in Equation (3), for $i \leq p$, the force function (F_F) is $2i - 1$, which will output the first p odd integers. This equation does not depend upon p, though p will determine how many joints are governed by this equation.

For $i > p$, the force function becomes more complex. While joint i is still crossed by and thus still receives contributions from muscles originating at more anterior joints, the muscles with anterior origins more than p away have terminated at their posterior insertions and thus no longer contribute (Fig. 2). For example, in a system with a span of $p = 3$, joint $i = 3$ is actuated by muscles originating on segments 1, 2, and 3, but joint $i = 4$ is actuated by muscles originating on segments 2, 3, and 4 (Fig. 2). Thus, the muscle which originates immediately anterior to the joint must now not only apply sufficient force to meet the increased external demand, but also compensate for the loss of the muscle which originated on joint $i-p$. This applies for all $i > p$, and results in $F_F(i, p)$ being defined by a piecewise equation:

$$F_F(i, p) = \begin{cases} 2i - 1 \ ; i \leq p \\ i^2 - \sum_{k=i-(p-1)}^{k=i-1} F_M(k, p) \ ; \ i > p \end{cases}. \quad (4)$$

The dependence of the value of $F_F(i, p)$ on values of F_F for a variable number of lower i values makes it cumbersome to deal with, though the force
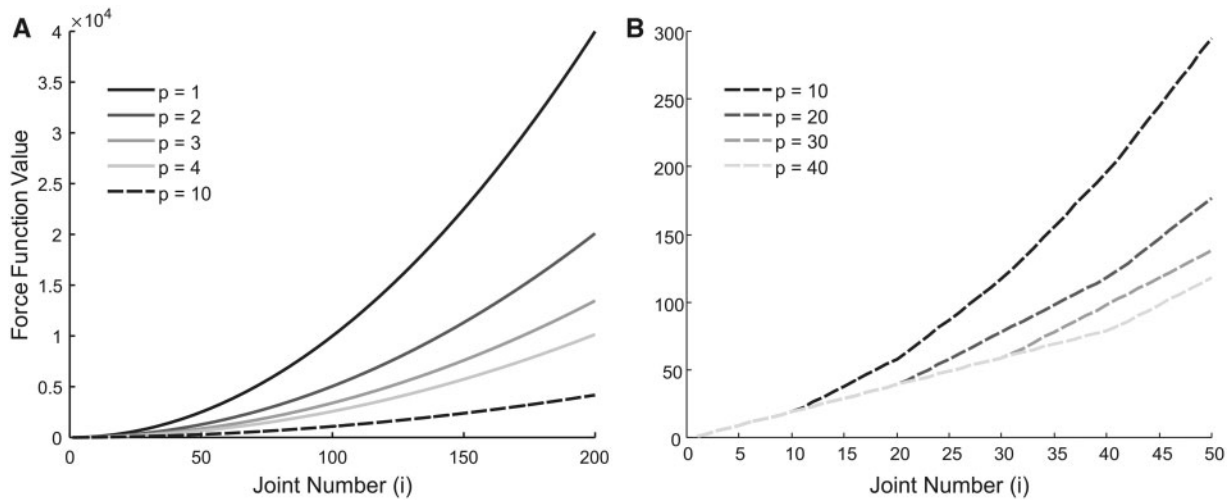
Fig. 3 Force function F_F (Equation (4)) versus i and p. (**A**) Force function value versus i for spans of 1–4 and 10. (**B**) Force function value versus i for spans of 10, 20, 30, and 40.

function can be readily computed with a simple computer program (Supplementary Code S1). From inspection of these results, it is clear that F_F decreases tremendously with p for any $i > p$, indicating that greater muscular span does indeed reduce the force needed in each muscle (Fig. 3).

While the force function is simply i^2 for $p = 1$ (due to equivalence with F_{Mtotal}/C_M), as p increases, it departs increasingly from the simple quadratic relation (Fig. 3). Furthermore, the curve of the force function for a given p is not actually a curve, but rather a series of line segments (Figs. 3B and 4). To progress further, this relationship must be approximated with a continuous function.

Upon closer inspection, the slope is constant for a length $p-1$, followed by a single segment with a slope 1 higher, followed by another series of length $p-1$ with a slope 2 higher than the previous one (Figs. 3B and 4). All slopes start at 2, and the segments of length $p-1$ are always even, with the intervening slopes of length 1 having odd slopes (Fig. 4A). Because the system is only valid at integer values of i and p, rather than an integral, the appropriate mechanism for calculating the "area under the curve" is summation rather than integration. Therefore, the pattern of slopes can be used to derive an approximation of $F_F(i, p)$:

$$F_F(i, p) = \left(\sum_{k=1}^{i/p} (2k-1) + (p-1) * \sum_{k=1}^{i/p} 2k \right). \quad (5)$$

Sum identities can be used to simplify Equation (5) to

$$F_F(i, p) = \left(\frac{i^2}{p} + \frac{p-1}{p} i \right). \quad (6)$$

This continuous equation approximates the explicit calculation, but intersects only at every pth point, otherwise under-predicting Equation (4) (Fig. 4B). Further inspection reveals that the maximum underprediction is $(p-1)^2/4p$, thus adjusting Equation (6) upward by adding half of this function yields

$$F_F(i, p) = \left(\frac{i^2}{p} + \frac{p-1}{p} i + \frac{(p-1)^2}{8p} \right). \quad (7)$$

The predicted values of this approximation were compared with the calculated values of Equation (4) for all values of p and i in $1 \leq p \leq 50$ and $1 \leq i \leq 200$, which showed that the force function has a maximum error of 6, corresponding to a mean relative error of only 3.5%, being higher at small i and p. However, these small values of i and p are of less biological relevance, and thus Equation (7) provides us with a highly accurate approximation for further computations. Previous work has attempted to link gap bridging performance to muscular anatomy using an approximation of $F_F(i, p)$ which assumed an even distribution of force across all muscles of a given segment (Jayne and Riley 2007). In that model, the contribution of any individual muscle is simply F_{Mtotal} (Equation (2)) divided by p. In Equation (7), there indeed is a term in the force function which matches this prediction, i^2/p. However, Equation (7) also includes a term which has a positive, linear relationship with i, showing that this "even activation
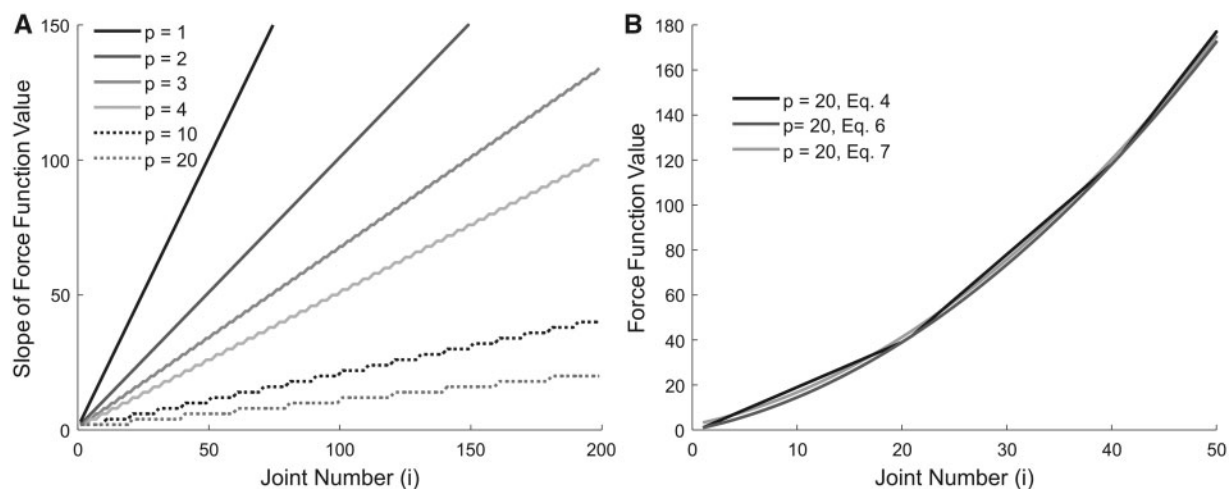
Fig. 4 Fitting a continuous function to Equation (4). (**A**) Slope of force function value (Equation (4), right side) for spans of 1–4, 10, and 20. Note that the slope increases discontinuously. (**B**) Force function value versus i for a span of 20, showing the results for Equations (4), (6), and (7). Note that Equation (6) underpredicts Equation (4) except where i is an integer multiple of p. Equation (7) adjusts Equation (6) upward to make these errors symmetrical.
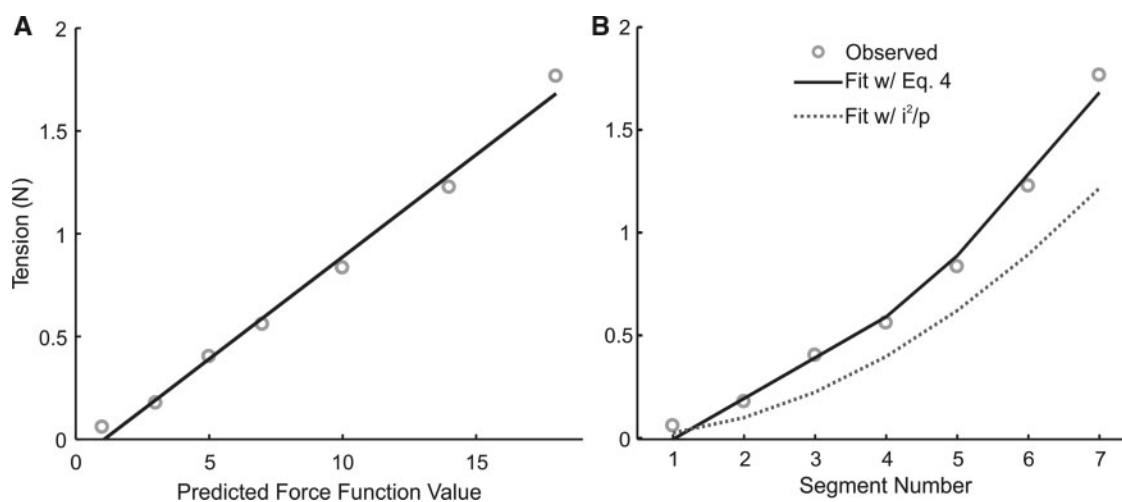
Fig. 5 Results of mechanical testing. (**A**) Predicted force function value from Equation (4) versus observed tension (gray circles). The black line indicates the linear regression (0.099 * (pred.)−0.10, $R^2 = 0.99$, $P < 0.0001$). The slope of this line corresponds to the morphological terms in Equation (4), C_M, which match predictions based on the model mass and geometry ($C_M = 0.10$). (**B**) Observed (gray circle) and predicted (black line) tension versus segment number, in contrast to predictions from a simple "even activation model" (dashed line).

model" will underestimate the actual force, and this underestimation will be greater for higher i and p. This can be observed even at small segment numbers (Fig. 5B).

Mechanical validation

The predicted forces for Equation (4) were tested using a mechanical model. A linear regression between force function (Equation (4), right side) and observed tension in MATLAB showed a highly significant linear fit ($R^2 = 0.99$, $p < 0.0001$) with a non-significant intercept and a slope of 0.099 (Fig. 5A).

The slope corresponds to the morphological coefficient (C_M) in Equation (4), and agrees closely with the value calculated from the segments directly (mass=6.54 g, length=5 cm, lever arm=1.6 cm, calculated $C_M = 0.10$ N).

Performance: maximum gap bridging

To determine the consequences of multi-articular span on maximum gap bridging performance, I determine the peak muscle force a single muscle is capable of generating, accounting for the subdivision
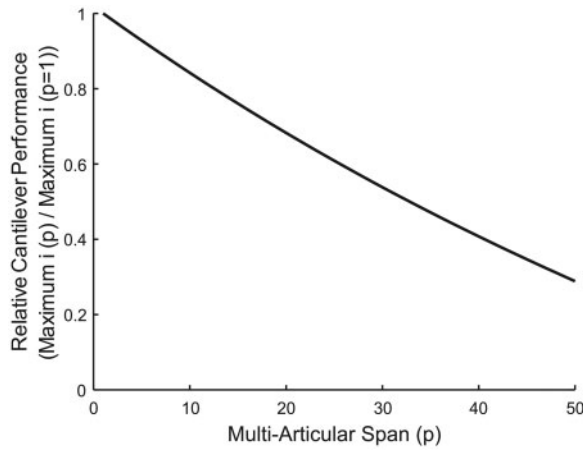
Fig. 6 Maximum cantilever performance (Equation (10)), expressed as a fraction of the performance for a mono-articular system, versus multi-articular span.

of the cross-sectional area into multi-articular "bundles" (see the section "Methods")

$$F_M(i,p) = P_0 \frac{\text{CSA}_{\max}}{p}$$
$$\geq \frac{m*g*L}{2*a} * \left(\frac{i^2}{p} + \frac{p-1}{p}i + \frac{(p-1)^2}{8p} \right), \quad (8)$$

which can be re-arranged into a simple quadratic form

$$0 \leq i^2 + (p-1)i + \frac{(p-1)^2}{8} - \frac{2*a*P_0*\text{CSA}_{\max}}{m*g*L} \quad (9)$$

and solved for i as a function of p via the quadratic formula

$$\text{Maximum } i(p) = \frac{-p+1 \pm \sqrt{\frac{(p-1)^2}{2} + \frac{8*a*P_0*\text{CSA}_{\max}}{m*g*L}}}{2}, \quad (10)$$

with the positive value of Equation (10) providing the maximum horizontal cantilever length in terms of p (negative values of Equation (10) are meaningless). Equation (10) can be evaluated for $1 \leq p \leq 50$ and arbitrary values of the various constants and divided by the result for $p = 1$ to see that increased multi-articular span decreases the maximum cantilever length (Fig. 6).

Careful inspection of the results of $F_F(i, p)$ (Equation (7); Fig. 3) reveals that, while increasing p reduces F_F at any $i > 1$, the reduction from $F_F(i, 1)$ to $F_F(i, p)$ is slightly less than the loss in cross-sectional area over that same interval. More formally, the partial derivative of Equation (10) with respect to p is

$$\frac{\partial(\text{Maximum } i(p))}{\partial p} = -\frac{1}{2} + \frac{p-1}{4*\sqrt{\frac{(p-1)^2}{2} + \frac{8*a*P_0*\text{CSA}_{\max}}{m*g*L}}} \quad (11)$$

which, because all morphological constants are positive, is negative for all $p > 0$, proving that increasing multi-articular span is always detrimental (Fig. 6). This result is strongly contrary to expectations, as increased multiarticular span is correlated with arboreality and thus gap bridging demands in the natural habitat.

To evaluate the consequence of tendons, which do not trade off against muscular cross-sectional area, I reformulate Equation (8) as

$$F_M(i,p,t) = P_0 \frac{\text{CSA}_{\max}}{(1-t)p}$$
$$\geq \frac{m*g*L}{2*a} * \left(\frac{i^2}{p} + \frac{p-1}{p}i + \frac{(p-1)^2}{8p} \right) \quad (12)$$

in which $(1-t) * p$ is the length of the muscular span, while $t * p$ is the tendinous span. This can be solved as above to express maximum gap spanned as function of both t and p

$$\text{Maximum } i(p,t) = \frac{-p+1 + \sqrt{\frac{(p-1)^2}{2} + \frac{8*a*P_0*\text{CSA}_{\max}}{m*g*L*(1-t)}}}{2}. \quad (13)$$

As previously, this can be graphed for arbitrary values of the assorted constants and expressed as a ratio of the value of $p = 1$, $t = 0$ to show that while increased span mildly decreases the maximum cantilever length, increased tendon ratio dramatically increases it (Fig. 7).

Partial derivatives with respect to both p and t show that maximal cantilever performance decreases for all increases of p for $p > 1$ (as above), but increases continuously for all $0 < t < 1$

$$\frac{\partial(\text{Maximum } i(p,t))}{\partial p} = -\frac{1}{2}$$
$$+ \frac{p-1}{4*\sqrt{\frac{(p-1)^2}{2} + \frac{8*a*P_0*\text{CSA}_{\max}}{m*g*L*(1-t)}}}, \quad (14)$$

$$\frac{\partial(\text{Maximum } i(p,t))}{\partial t} = \frac{\frac{2*a*P_0*\text{CSA}_{\max}}{m*g*L}}{\sqrt{\frac{(1-t)(p-1)^2}{2} + \frac{8*a*P_0*\text{CSA}_{\max}}{m*g*L}}}. \quad (15)$$

Solving for the minimum t necessary to offset the detriment due to increased p (relative to 1) yields
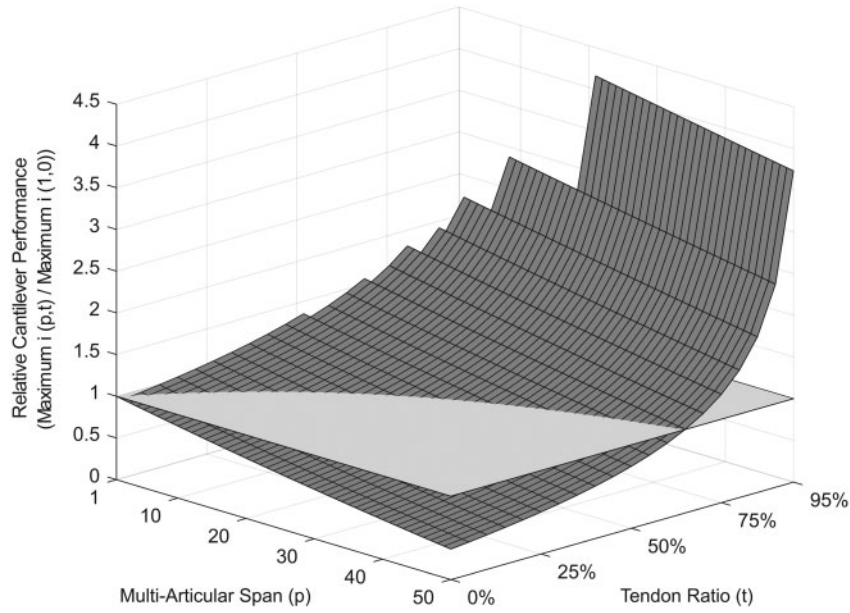
Fig. 7 Maximum cantilever performance (Equation (13)), expressed as a fraction of the performance for a mono-articular, purely muscular system, versus multi-articular span and tendon ratio. The plane is at 1, indicating that combinations of p and t above the plane will have performance superior to the mono-articular, muscular system.
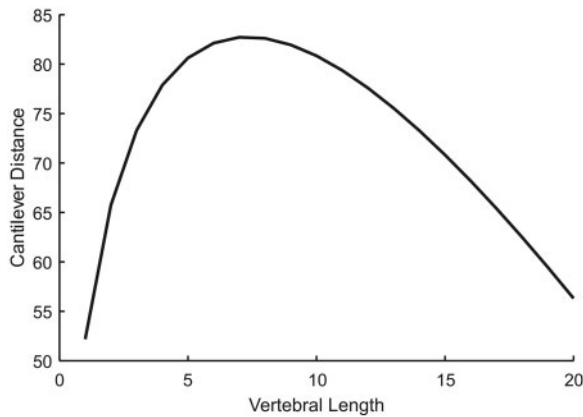
Fig. 8 Cantilever distance versus vertebral length (Equation (17)). For any set of morphological parameters, span, and tendon ratio, there exists an optimal vertebral length (Equation (18)), beyond which cantilever distance declines (Equation (19)). Units of both axes are arbitrary.

Minimum Tendon Ratio $(p) \geq 1 - \dfrac{A}{\left(p + \sqrt{A} - 1\right)^2 - \frac{(p-1)^2}{2}}$,

where $A = \dfrac{8*a*P_0*\mathrm{CSA_{max}}}{m*g*L}$,

where A is a combination of the morphological and physiological constants, showing that relatively little tendon is required in order to "break even" (Fig. 7). As A increases, representing either increased strength and leverage or reduced load, the required tendon ratio decreases.

While most morphological constants in Equation (13) behave as expected, increased segment length (L) will decrease maximum number of segments which can be cantilevered, but increase the absolute distance. To examine this tradeoff, I compute the maximum horizontal cantilever distance in absolute length as the product of the maximum number of joints and the segment length

$$\text{Cantilever Distance } (p,t,L) = L * \text{Max. } i(p,t)$$
$$= \frac{-p*L + L + L\sqrt{\frac{(p-1)^2}{2} + \frac{8*a*P_0*\mathrm{CSA_{max}}}{m*g*L*(1-t)}}}{2}. \quad (17)$$

If increasing L increases cantilever distance, the derivative of Equation (17) with respect to L must be greater than zero

$$\frac{\partial(\text{Cantilever Distance } (p,t,L))}{\partial L}$$
$$= \frac{-p}{2} + \frac{1}{2} + \frac{(p-1)^2 L + \frac{8*a*P_0*\mathrm{CSA_{max}}}{m*g*(1-t)}}{4\sqrt{\frac{(p-1)^2 L^2}{2} + L * \frac{8*a*P_0*\mathrm{CSA_{max}}}{m*g*(1-t)}}} > 0, \quad (18)$$

which can be satisfied when

$$L < \frac{(\sqrt{2}-1)8*a*P_0*\mathrm{CSA_{max}}}{m*g*(1-t)*(p-1)^2} \quad (19)$$

showing that there is indeed a limit to L, beyond which increased vertebral segment length will cause decreases in cantilever performance (Fig. 8). As coefficients related to strength and muscular moment
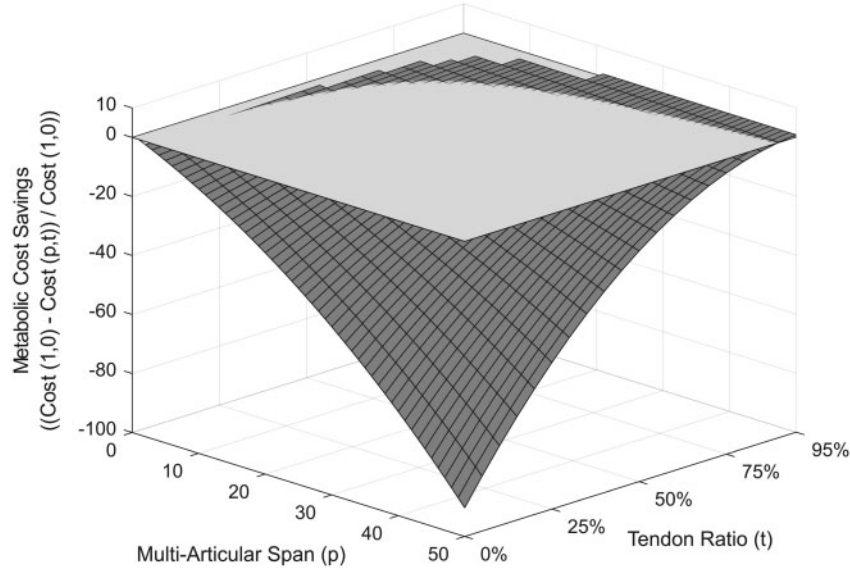
Fig. 9 Metabolic cost savings vs. multi-articular span (*p*) and tendon ratio (*t*) at a gap of $i = 100$, expressed as the reduction in cost below that of a mono-articular, purely muscular system, and divided by this same reference value (based on Equation (23)). A value of 0.5 represents a 50% reduction in metabolic cost. Negative values represent increased metabolic cost. For all but the most tendinous systems, the metabolic cost is dramatically higher than a mono-articular, purely muscular system. This minimum margin is lower at lower gap lengths (Supplementary Material S2).

(P_0, CSA_{max}, and *a*) increase and as coefficients related to load decrease (*m* and *g*), this limit rises. As with overall performance, increased multiarticular span causes the maximum beneficial vertebral length to decline, while this length increases with increasing tendon ratio.

Metabolic cost

The metabolic cost of a single muscle in our system is proportional to the volume of active muscle tissue.

$$\text{Metabolic Cost per muscle } (p, t) = CSA * p * L * (1 - t) * Q, \tag{20}$$

where *Q* is a constant representing the cost of isometrically activating a given volume of muscle. However, for submaximal loads, muscle will only need to activate a portion of the total cross-sectional area available. To determine the required cross-sectional area for a given muscle, Equation (12) is reformulated to solve for cross-sectional area at a given *i*, *p*, and *t*.

$$\text{Required CSA } (i, p, t) = \frac{m * g * L * (1 - t)}{2 * a * P_0} \\ * \left(i^2 + (p - 1)i + \frac{(p - 1)^2}{8} \right), \tag{21}$$

which can be combined with Equation (20) to yield a metabolic cost equation of

Metabolic Cost per muscle (i, p, t)

$$= \frac{p * Q * m * g * L^2 * (1 - t)^2}{2 * a * P_0} * \left(i^2 + (p - 1)i + \frac{(p - 1)^2}{8} \right). \tag{22}$$

This can be summed over the interval from 1 to *i* to give total cost of

Total Metabolic Cost (i, p, t)

$$= \frac{p * Q * m * g * L^2 * (1 - t)^2}{2 * a * P_0} * \left(\frac{i^3}{3} + \frac{p * i^2}{2} + \left(\frac{3p^2 + 6p - 5}{24} \right) i \right) \tag{23}$$

based on distributivity, associativity, and sum identities (Supplementary Material S2). As would be expected, longer cantilever distances (increasing *i*) result in increasing cost, since required forces rise and more muscles must become involved. Partial derivatives with respect to each of the variables show that metabolic cost increases with both *i* and *p*, but decreases with *t* (Supplementary Material S2).

The nature of these relationships becomes clear when metabolic cost is graphed as a function of multi-articular span and tendon ratio for a given cantilever length relative to the cost of a purely muscular, mono-articular system (Fig. 9). The tendon ratio at which the metabolic cost of a given mutli-articular span decreases below that for the purely muscular, mono-articular system is very high at high cantilever distances (high values of *i*), but

increases only modestly with span ([Fig. 9](#) and [Supplementary Material](#) S2).

Range of motion

Consider a segment of the snake's vertebral column which is of uniform curvature k (defined as the inverse of the radius of curvature R) with a muscle at constant lever arm a. The vertebral column will be considered incompressible and of length L_{vert}, and thus this arc of curvature k will subtend an angle of θ (in radians) such that $L_{vert}=R * \theta$. Because θ must be the same for the muscle and the vertebral column, the length of the muscle on the inner side of the arc will be $L_{in}=(R-a) * \theta$. Since, when straight, both muscles will be equal in length to the segment of the vertebral column ($L_{vert}=L_{in}$), the strains for each muscle is

$$\text{Strain}_{inner} = \frac{L_{vert} - L_{in}}{L_{vert}} = \frac{R*\theta - (R-a)*\theta}{R*\theta} = \frac{a}{R} = a*k \tag{24}$$

if the straight position is regarded as the "neutral" length. A similar derivation can show that the strain of the outer muscle is also $a * k$. Therefore if, during a locomotor cycle, the segment was to start at curvature k, straighten, and continue to bend to the opposite side to the same curvature k, the muscle would undergo a total strain of $2*a*k$. Crucially, because this is a relative measurement of percentage shortening, it remains constant regardless of how many vertebral and muscular segments are in the arc (as shown by the lack of a θ, L_{vert}, or L_{in} term in [Equation (24)](#)). Thus multi-articular span has no effect on either the relative length change of a fiber or the relative contractile velocity, provided that the entire region is of constant curvature.

For extremely large multi-articular span, this may not be the case. Because snakes have highly variable numbers of vertebrae, the multiarticular span of a given muscle may span anywhere from 4% to 22% of the total body vertebrae ([Jayne 1982](#)). Because local strain is only a function of lever arm and curvature of an arc, a snake can be represented parametrically as a smooth curve from position 1 (the head) to position s (the tip of the tail), with curvature at all points along the body as a function of s, $k(s)$. Correspondingly, the strain of any multiarticular muscle spanning two locations on the snake would be the definite integral of the curvature function $k(s)$ over the given body segment, with negative values of curvature denoting curves to one side and positive values to the other, multiplied by the lever arm and divided by the length of the integral region.

However, while snakes approximate smooth curves, their axial system is ultimately comprised of rigid segments separated by discrete joints. For vertebrae of length L, the arc connecting the midpoint of each vertebra (distance $L/2$ from the joint) and the center of rotation of the joint between them has a curvature of

$$k = \frac{4*\sin\left(\frac{\beta}{2}\right)}{L} \xrightarrow[\text{small angle approx.}]{} \frac{2*\beta}{L}, \tag{25}$$

where β is the angle between the two vertebrae. The small angle approximation reduces this to a simpler form (provided the angle is computed in radians), and yields 98% accuracy within the range of motion typical of snake vertebrae ([Jayne 1988a](#); [Sharpe et al. 2015](#); [Morinaga and Bergmann 2019](#); [Jurestovsky et al. 2020](#)). Therefore, strain can be expressed as a function of intervertebral joint angle, vertebral length, and lever arm

$$\text{Strain} = \frac{2*a*\beta}{L}. \tag{26}$$

However, because tendon changes length relatively little, increased tendon ratio will require that the length change be achieved only by the muscular portion of the muscle–tendon unit

$$\text{Strain} = \frac{2*a*\beta}{L*(1-t)}. \tag{27}$$

Thus, as tendon ratio increase, the range of vertebral motion for a given allowable muscle fascicle strain range decreases. Correspondingly, increasing t requires that the muscle strain and strain rate for a given curvature and rate of curvature change increases.

Discussion

These derivations above provide the first detailed look into the mechanics of multi-articular muscle systems at the individual muscle level. For our target behavior, cantilevered gap bridging, I was able to show that increasing the span of purely muscular multi-articular systems result in a modest performance decrease, but increasing the tendon ratio for a given span produced large gains in gap bridging performance. In contrast, metabolic cost was usually higher than mono-articular, purely muscular systems except for a very few, highly tendinous configurations. Range of motion was unaffected multiarticular span itself, but was adversely affected by increased tendon ratio.
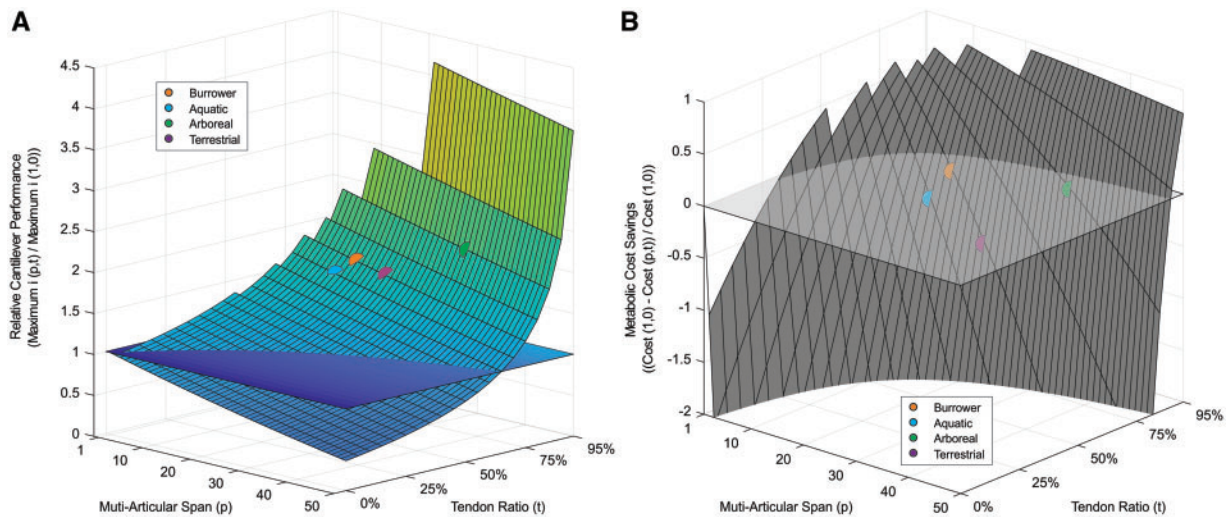
Fig. 10 Caenophidian snake data plotted on performance and metabolic cost surfaces (Figs. 7 and 9). Values of multi-articular span and tendon ratio were computed from Table 4 of Jayne (1982). Constrictors and non-constrictors were merged due to the closeness of the points. (**A**) Performance of biological snakes when compared with a hypothetical, mono-articular purely muscular system. Horizontal plane indicates a value of 1, equal to this baseline. Burrowing, aquatic, and terrestrial snakes show similar improvements over the mono-articular systems (1.8, 1.6, and 1.7, respectively), while arboreal species showed an improvement of 2.1. (**B**) Metabolic cost savings for a gap of $i = 100$, when compared with a hypothetical, mono-articular, purely muscular system. Horizontal plane indicates a value of 1, equal to this baseline. All species showed negative values, indicating greater metabolic cost than a mono-articular, purely muscular system, though they are close to the margin (burrowing = 14% higher cost, aquatic = 38% higher cost, terrestrial = 72% higher cost, and arboreal = 13% higher cost).

Biological context

Based on these results, the observed values of snake SSP multi-articular span and tendon ratio can be mapped onto the performance spaces for maximum perfornace and metabolic cost. Because the snake SSP varies not just in multi-articular span and tendon ratio but also relevant morphological variables such as vertebral length, mass, muscle cross-sectional area, and lever arm (Equations (13) and (20)), it is difficult to compare species directly. However, this can be mitigated by computing the ratio between the computed values for a given multi-articular span and tendon ratio and the value for mono-articular muscles with no tendon, as previously in the results. As a result, a given value is not the snake's actual performance, but rather a metric of how much their multi-articular span and tendon ratio improves their performance beyond this hypothetical baseline. To avoid confounding the consequences of greater cantilever performance with metabolic cost, as increased number of joints in the cantilevered body segment must lead to increased metabolic cost, metabolic cost was evaluated at a standard cantilever performance of $i = 100$ (Fig. 10B). Values of multi-articular span and tendon ratio were computed from Table 4 of Jayne (1982).

These values show that snakes with the mean morphology of each habitat cluster display elevated performance relative to the alternative of a hypothetical, mono-articular purely muscular system (Fig. 10A). This is largely due to the combination of multi-articular anatomy and high tendon ratio, even for burrowers and aquatic species (Fig. 10A). Examination of data for individual snake species (Jayne 1982) showed that most would be fairly close to the center of their clusters. The differences computed, however, are far less substantial than the observed differences in cantilever gap bridging performance (Lillywhite et al. 2000; Ray 2012), showing that morphological variables likely play a large role in cantilever performance.

In contrast, the metabolic cost was greater in configurations observed in real snakes than for the hypothetical mono-articular purely muscular system. However, biological values were very close to the plane of equality (Fig. 10B), suggesting that selection pressure for metabolic economy may still occur. These calculations also assumed a relatively simple model for metabolic cost (proportional to active muscle volume) while the real cost is likely more complex. However, this behavior is also likely to be subject to greater selection for performance than economy, and thus these results are not entirely surprising. The data on increased vertebral length aligns well with biological data, in which arboreal snakes with long, highly tendinous SSP muscles also have

relatively elongate vertebrae (Lawing et al. 2012), but not nearly so dramatic an elongation as in other taxa (Li et al. 2004).

The notable tradeoff with range of motion also corresponds well with biological data, though range of motion is known only for a few species (Jurestovsky et al. 2020). Dorsoventral range of motion is approximately 20° (less than half of the lateral range of motion) and is greater ventrally than dorsally (dorsal ROM=8.9–11.3°) (Jurestovsky et al. 2020), suggesting the highly tendinous SSP limits range of motion and requires large muscle fiber length changes for relatively small movements. Whether this increased strain and contractile velocity is beneficial is likely to depend on both the function and the contractile properties of the muscle (Ruben 1977). While muscular lever arms have never been quantified in snakes, length:width ratios from a dorsal view are reported as ranging from about 0.5 to 1 (Lawing et al. 2012). Range of motion has only been quantified in a few snakes, but is approximately 0.3 radians dorsoventrally (total) and 0.3 radians laterally (straight to maximum joint angle) (Jayne 1988a; Sharpe et al. 2015; Jurestovsky et al. 2020). For a hypothetical constrictor using maximal lateral bending, a muscle with no tendon inserting on the most lateral tip of the pre- and post-zygapophysis would need to operate across a strain range of 30–60% (to account for bending to each side); muscles inserting on the ribs would be subject to even greater strains. These strains are possible but are on the high end of the range of reported muscle strain values (Burkholder and Lieber 2001). Alternatively, laterally undulating snakes typically use substantially less than the limit of their range of motion, but rarely exceed locomotor frequencies of 2 Hz (Jayne 1986), suggesting muscle contractile velocities of substantially less than 1 length per second. While no data exists on the force velocity relationship of snake muscle, this is far below the speeds which yield peak power for any vertebrate locomotor muscle at physiologically relevant temperatures (Hill 1938; Woledge 1968; Askew and Marsh 2002; Roberts et al. 2011; Astley 2016). Increasing tendon ratio for the muscle would result in corresponding increases in strain rate, allowing muscles to operate closer to optimally for peak isotonic power, at the cost of range of motion and the need to traverse a broader range of the length–tension curve.

Alternative loading regimes

The above calculations and results are limited to a simple, horizontally cantilevered snake, but the methods followed could be applied to any alternative loading regime: a gap-bridging snake supported at two points ("simply supported" in engineering terms), a snake moving horizontally on a frictional plane, a snake on a horizontal plane pressing against one or more pegs, etc. Indeed, if there exist enough conditions to make this analysis solvable, the external moments (Equation (1)) could be any arbitrary continuous function. The results of this paper, such as that multi-articular span requires a tendinous component to be beneficial, may not hold for these conditions. Far from undermining this paper, this may explain why different muscles in the snake axial system have such tremendous differences is span and tendon ratio (Fig. 1), or elucidate the mechanical basis for tradeoffs between various behaviors (e.g., constriction vs. lateral undulation speed).

Robots

These findings have applications beyond biological snakes, particularly with regard to snake robots, and indeed most prior mechanistic analysis of these systems has been with the goal of adapting it to robots to improve their performance (Rezaei et al. 2010; Kano et al. 2011; Faraji and Barazandeh 2012). Snake robots significantly under-perform compared with biological snakes, particularly when considering the relatively large portion of their mass dedicated to motors, and multi-articular muscles may improve their performance and help close this gap (Kano et al. 2011). Because most snake robots are typically actuated by electric motors, which function primarily in rotation (e.g., DC motors and servomotors), multi-articular systems would likely confine the motor to a single joint, with the remaining span accomplished via cables, producing an analog of a very high tendon ratio and eliminating the tradeoff between span and force seen in Equation (8). Unlike muscle, which has a limited length change, motors capable of indefinite rotation, such as DC motors, would face no tradeoff with range of motion, though motors still face a tradeoff between torque and rpm that is analogous to the muscle force–velocity relationship. Finally, unlike muscles, in which increased fiber length will increase metabolic cost (Equation (20)) (Biewener and Roberts 2000), electrical current is directly proportional to torque, so any anatomy which reduces mechanical loading will also reduce electrical power. While current snake robots are rather slow and cumbersome compared with the speed and elegance of their biological counterparts, the implementation of multi-articular morphology

may allow increased performance, albeit potentially at the cost of control complexity.

Conclusions

By using a mathematical model of horizontal cantilevering behavior in snakes, I was able to show that increased multi-articular muscle span improved both maximum cantilever performance and metabolic savings, but only if a substantial fraction of that span is tendinous. These results corresponded well with anatomical studies of snakes (Jayne 1982; Tingle et al. 2017) and previous robotic studies (Kano et al. 2011), and open the door for both a deeper understanding of how snake muscular morphology corresponds to locomotor performance and the potential for improved biomimetic snake robots. However, many open questions remain in these areas, representing a rich area of future research.

Supplementary data

Supplementary data are available at *ICB* online.

References

Astley HC. 2016. The diversity and evolution of locomotor muscle properties in anurans. J Exp Biol 2193163–73.

Askew GN, Marsh RL. 2002. Muscle designed for maximum short-term power output: quail flight muscle. J Exp Biol 205:2153–60.

Auffenberg W. 1962. A review of the trunk musculature in the limbless land vertebrates. Am Zool 2:183–90.

Bedford A, Fowler WL, Morris E. 1997. Statics: engineering mechanics. Reading, Massachusetts: Addison-Wesley.

Biewener AA, Roberts TJ. 2000. Muscle and tendon contributions to force, work, and elastic energy savings: a comparative perspective. Exerc Sport Sci Rev 28:99–107.

Bodine SC, Roy RR, Meadows DA, Zernicke RF, Sacks RD, Fournier M, Edgerton VR. 1982. Architectural, histochemical, and contractile characteristics of a unique biarticular muscle: the cat semitendinosus. J Neurophysiol 48:192–201.

Böhmer C, Prevoteau J, Duriez O, Abourachid A. 2019. Gulper, ripper and scrapper: anatomy of the neck in three species of vultures. J Anat pubished online (doi: 10.1111/joa.13129).

Boumans M, Krings M, Wagner H. 2015. Muscular arrangement and muscle attachment sites in the cervical region of the American barn owl (*Tyto furcata pratincola*). PLoS ONE 10:e0134272.

Burkholder TJ, Lieber RL. 2001. Sarcomere length operating range of vertebrate muscles during movement. J Exp Biol 204:1529–36.

Daggfeldt K, Thorstensson A. 2003. The mechanics of back-extensor torque production about the lumbar spine. J Biomech 36:815–25.

Faraji H, Barazandeh F. 2012. Analysis and simulation of a snake robot based on muscles and vertebrae anatomy of snake. Proc Inst Mech Eng Part K J Multi-body Dyn 226:17–25.

Fowler N, Nicol A, Condon B, Hadley D. 2001. Method of determination of three dimensional index finger moment arms and tendon lines of action using high resolution MRI scans. J Biomech 34:791–7.

Gasc J-P. 1974. L'interpretation fonctionelle de l'appareil musculosquelettique de l'axe serpentiformes. Mem Mus Natl Hist Nat 48:69–124.

Gasc JP. 1981. Axial musculature. In: Gans C, Parsons TS, editors. Biology of the reptilia. New York (NY): Academic Press. p. 355–435.

Inoue K, Nakamura K, Suzuki M, Mori Y, Fukuoka Y, Shiroma N. 2010. Biological system models reproducing snakes' musculoskeletal system. IEEE/RSJ 2010 International Conference on Intelligent Robots and Systems, IROS 2010—Conference Proceedings. p. 2383–8.

Jayne BC. 1986. Kinematics of terrestrial snake locomotion. Copeia 1986:195–208.

Jayne BC. 1982. Comparative morphology of the semispinalis-spinalis muscle of snakes and correlations with locomotion and constriction. J Morphol 172:83–96.

Jayne BC. 1988a. Muscular mechanisms of snake locomotion: an electromyographic study of the sidewinding and concertina modes of *Crotalus cerastes*, *Nerodia fasciata* and *Elaphe obsoleta*. J Exp Biol 140:1–33.

Jayne BC. 1988b. Muscular mechanisms of snake locomotion: an electromyographic study of lateral undulation of the Florida banded water snake (Nerodiafasciata) and the yellow rat snake (Elapheobsoleta). J Morphol 197:159–81.

Jayne BC, Riley MA. 2007. Scaling of the axial morphology and gap-bridging ability of the brown tree snake, *Boiga irregularis*. J Exp Biol 210:1148–60.

Johnson RG. 1955. The adaptive and phylogenetic significance of vertebral form in snakes. Evolution (NY) 9:367–88.

Jorgensen RM, Jayne BC. 2017. Three-dimensional trajectories affect the epaxial muscle activity of arboreal snakes crossing gaps. J Exp Biol 220:3545–55.

Jurestovsky DJ, Jayne BC, Astley HC. 2020. Experimental modification of morphology reveals the effects of the zygosphene–zygantrum joint on the range of motion of snake vertebrae. J Exp Biol 223:jeb216531.

Kano T, Sato T, Kobayashi R, Ishiguro A. 2011. Decentralized control of multi-articular snake-like robot for efficient locomotion. Institute of Electrical and Electronics Engineers (IEEE). p. 1875–80.

Lawing AM, Head JJ, Polly PD. 2012. The ecology of morphology: The ecometrics of locomotion and macroenvironment in North American snakes. In: Louys J, editor. Paleontology in ecology and conservation. Berlin, Heidelberg: Springer. p. 117–46.

Lemelin P. 1995. Comparative and functional myology of the prehensile tail in new world monkeys. J Morphol 224:351–68.

Li C, Rieppel O, LaBarbera MC. 2004. A triassic aquatic protorosaur with an extremely long neck. Science 305:1931.

Lillywhite HB, LaFrentz JR, Lin YC, Tu MC. 2000. The cantilever abilities of snakes. J Herpetol 34:523.

Macintosh JE, Bogduk N, Pearcy MJ. 1993. The effects of flexion on the geometry and actions of the lumbar erector spinae. Spine (Phila Pa 1976) 18:884–93.

Mccartney JA. 2013. Morphology and function of the ophidian vertebral column: implications for the paleobiology of fossil snakes (http://hdl.handle.net/11401/77243).

Morinaga G, Bergmann PJ. 2019. Angles and waves: intervertebral joint angles and axial kinematics of limbed lizards, limbless lizards, and snakes. Zoology 134:16–26.

Mosauer W. 1935. The myology of the trunk region of snakes and its significance for ophidian taxonomy and phylogeny. Publ Univ Calif Los Angeles Biol Sci 1:81–120.

Penning DA. 2018. Quantitative axial myology in two constricting snakes: *lampropeltis holbrooki* and *Pantherophis obsoletus*. J Anat 232:1016–24.

Pollard NS, Gilbert RC. 2002. Tendon arrangement and muscle force requirements for human-like force capabilities in a robotic finger. Proceedings 2002 IEEE International Conference on Robotics and Automation IEEE. p. 3755–62.

Pregill GK. 1977. Axial myology of the racer coluberconstrictor with emphasis on the neck region. Trans San Diego Soc Nat Hist 18:185–206.

Ray JM. 2012. Bridging the gap: interspecific differences in cantilevering ability in a neotropical arboreal snake assemblage. South Am J Herpetol 7:35–40.

Rezaei SM, Barazandeh F, Haidarzadeh MS, Sadat SM. 2010. The effect of snake muscular system on actuators' torque. J Intell Robot Syst 59:299–318.

Roberts TJ, Abbott EM, Azizi E. 2011. The weak link: do muscle properties determine locomotor performance in frogs? Philos Trans R Soc B 366:1488–95.

Ruben JA. 1977. Morphological correlates of predatory modes in the coachwhip (*Masticophis flagellum*) and rosy boa (*Lichanura roseofusca*). Herpetologica 33:1–6.

Sharpe SS, Koehler SA, Kuckuk RM, Serrano M, Vela PA, Mendelson J, Goldman DI. 2015. Locomotor benefits of being a slender and slick sand-swimmer. J Exp Biol 218:440–50.

Smith JM, Savage R. 1956. Some locomotory adaptations in mammals. Zool J Linn Soc 42:603–22.

Tingle JL, Gartner GEA, Jayne BC, Garland T. 2017. Ecological and phylogenetic variability in the spinalis muscle of snakes. J Evol Biol 30:2031–43.

Tveit P, Daggfeldt K, Hetland S, Thorstensson A. 1994. Erector spinae lever arm length variations with changes in spinal curvature. Spine (Phila Pa 1976) 19:199–204.

van der Leeuw AHJ, Bout RG, Zweers GA. 2001. Control of the cranio-cervical system during feeding in birds. Am Zool 41:1352–63.

Van Ingen Schenau GJ. 1989. From rotation to translation: constraints on multi-joint movements and the unique action of bi-articular muscles. Hum Mov Sci 8:301–37.

van Ingen Schenau GJ, Pratt CA, Macpherson JM. 1994. Differential use and control of mono- and biarticular muscles. Hum Mov Sci 13:495–517.

Winchester L, Bellairs A. 2009. Aspects of vertebral development in lizards and snakes. J Zool 181:495–525.

Winter DA. 2009. Biomechanics and motor control of human movement. 4th ed. Hoboken (NJ): John Wiley & Sons, Inc.